Tertiary Structural Changes in the Cleft Containing the ATP Sensitive Tryptophan and Reactive Thiol Are Consistent with Pivoting of the Myosin Heavy Chain at Gly699[†]

Thomas P. Burghardt,* Susanna P. Garamszegi, Sungjo Park, and Katalin Ajtai

Department of Biochemistry and Molecular Biology, Mayo Foundation, Rochester, Minnesota 55905

Received January 5, 1998; Revised Manuscript Received March 25, 1998

ABSTRACT: The conformation of myosin subfragment 1 (S1) in the vicinity of the ATP sensitive tryptophan (Trp510) and the highly reactive thiol (SH1), both residing in the "probe-binding" cleft at the junction of the catalytic and lever arm domains, was studied to ascertain its role in the mechanism of energy transduction and force generation. In glycerinated muscle fibers in rigor, a fluorescent probe linked to SH1 detects a strained probe-binding cleft conformation following a length transient by altering emission intensity without detectably rotating. In myosin S1 in solution, the optical activity of Trp510 senses conformation change in the probe-binding cleft caused by substrate analog trapping of S1 in various structures attainable transiently during normal energy transduction. Also in S1 in solution, the induced optical activity of a fluorescein probe linked to SH1 shows sensitivity to changing probe-binding cleft conformation caused by nucleotide binding to the S1 active site. The changes in the optical activity of Trp510 and SH1 bound fluorescein in response to nucleotide or nucleotide analog binding are interpreted structurally using the S1 crystallographic coordinates and aided by a model of energy transduction that pivots at Gly699 to change probe-binding cleft conformation and to displace the S1 lever arm as during force generation. The crystallographic structure of the probe-binding cleft in S1 resembles most the nucleotide bound conformation in the native protein. A different structure, generated by pivoting at Gly699, better resembles the native rigor conformation of the probe-binding cleft. Pivoting at Gly699 rotates probes at SH1 suggesting that length transients on fibers in rigor do not cause pivoting at Gly699 or reverse the power stroke.

The rotating myosin cross-bridge model of contraction in muscle gives a framework for investigating the transduction of free energy from ATP hydrolysis into work (*1*−*3*). The model provides for work production with the repetitive delivery of impulses to the actin filament by independently acting myosin cross-bridges. These cross-bridges bind and hydrolyze ATP, strongly bind actin, rotate, then repeat the cycle. The investigation of the structural changes within the enzymatic domain of the myosin cross-bridge (subfragment 1 or S1) that carry out this function center on the site of hydrolysis (active site) and pathways emanating from there to the actin binding site, the "probe-binding cleft" containing an ATP sensitive tryptophan (Trp510[1]) and highly reactive thiol (Cys707 or SH1), and other sites believed to participate in work production (*4*). Myosin's binding site for actin has an affinity that depends on the substrate in its active site and was proposed as the place where torque is generated to rotate the actin bound cross-bridge (*5*). Alternatively, an articulated cross-bridge consisting of a fixed globular catalytic/actin-binding domain and a rotating lever arm domain was proposed on the basis of the analogy between the crystallographic structures of S1 and adenylate kinase (*6*). Consistent with the latter proposal is the opening and closing of a cleft at the junction of the catalytic and lever arm domains, possibly at the probe-binding cleft.

Nonhydrolyzable nucleotide analogs mimicking transient substrates of ATPase tightly bind to the active site of S1 and trap the protein in various structures attained only transiently during normal energy transduction (*7*). The varying dynamic acrylamide quenching constant of Trp510 fluorescence as a function of bound nucleotide analog suggested that the probe-binding cleft closes incrementally during the splitting of ATP from its most open conformation obtained in the absence of substrate (*8*). This action appears to be driven at least in part by the incremental elongation of the covalent bonds connecting the $\gamma-$ and β-phosphates of the ATP substrate during hydrolysis (*9*) and may also involve the accompanying change in γ-phosphate coordination geometry (*10*, *11*). The movement in the probe-binding cleft during energy transduction, viewed in terms of the rotating cross-bridge model of contraction, might follow a script

[†] This work was supported by the National Institutes of Health Grant AR39288 and by the Mayo Foundation.

[1] Abbreviations: Cys707 or SH1, myosin most reactive thiol; DHNBS, dimethyl(2-hydroxy-5-nitrobenzyl)sulfonium bromide; D-S1, DHNBS modified myosin subfragment 1; DTNB, 5,5′-dithiobis(2-nitrobenzoate); DTT, dithiothreitol; EGTA, ethylene glycol bis(β-aminoethyl ether)-*N*,*N*,*N*′,*N*′-tetraacetic acid; (FD)CD, (fluorescence detected)circular dichroism; FRET, fluorescence resonance energy transfer; PMSF, phenylmethanesulfonyl fluoride; Trp131(510), tryptophan 131(510) in chicken pectoralis muscle myosin sequence; UV, ultraviolet; 5′F-S1, 5′iodoacetamidofluorescein labeled S1; 5′IAF, 5′iodoacetamidofluorescein; 5′IATR(-S1), 5′ isomer iodoacetamidotetramethylrhodamine (modified S1).

S0006-2960(98)00015-4 CCC: $15.00
Published on Web 05/08/1998

wherein a detached or weakly actin bound cross-bridge hydrolyzes ATP and closes the probe-binding cleft then forms a strong actin bond and provides the impulsive force while the cleft opens to its conformation in the absence of nucleotide. In this picture the lever arm is rotating relative to the catalytic domain while the probe-binding site is closing then opening.

Lever arm movement, with fixed catalytic domain, introduces flexibility requirements on the myosin heavy chain possibly involving the pivoting of the peptide backbone at the highly conserved glycine residue Gly699. Consistent with this suggestion was the inhibition of actin sliding velocity by replacement of Gly699 with a residue having a larger side chain to sterically restrict pivoting about the residue's Ramachandran angles (*12*). Conformation changes in the probe-binding cleft, affecting accessibility of Trp510 to quencher and other observable properties described below, as well as the movement of the lever arm of myosin, can be accomplished by the pivoting of the peptide at Gly699. We use this mechanism to model myosin structural changes accompanying hydrolysis that affect observable properties of the probe-binding cleft.

We present here experimental findings on the conformation of the probe-binding cleft during energy transduction from myosin assembled in a muscle fibers or when isolated in solution. Glycerinated muscle fibers were specifically modified with the fluorescent probe 5′iodoacetamidofluorescein (5′IAF) at Cys707 and fluorescence intensity detected during length transients applied to the fiber in rigor. Increasing tension on the rigor cross-bridges decreased probe emission intensity while producing no detectable probe rotation. Probe emission intensity follows tension development in the rigor fiber during the length transient. The change in 5′IAF emission intensity produced by the length transient indicates a strain induced conformation change in the probe-binding cleft. Earlier work showed enhanced fluorescence emission from 5′IAF modified S1 (5′F-S1) when actin bound in a rigor complex suggesting that the open conformation of the probe-binding cleft reduces probe quenching by reducing interaction with a tryptophan side chain (*13, 14*). Trp510 closely interacts with 5′IAF modified Cys707 and is certainly a quencher of the probe emission (*15*). Our present data suggests that strain induced in the cross-bridge by pulling on the rigor fiber increases the ability of Trp510 to quench the fluorescein probe.

The location of Trp510 makes it a potential intrinsic probe of the tertiary structure of the probe-binding cleft. The near-ultraviolet (UV) circular dichroism (CD) signal from a tryptophan residue in a protein senses the conformation of the side chain by detecting local interactions of indole with the peptide backbone and other aromatic residues. These interactions can be modeled and used to calculate the rotary strength of the tryptophan CD spectrum from a protein structure (*16, 17*). We isolated and quantified the shape and relative intensity of the Trp510 CD signal in S1, as a function of substrate in its active site, using fluorescence detected circular dichroism (FDCD) (*18*). Model calculations, based on the crystallographic structure of S1 (*6*) and its alteration by pivoting the lever arm at Gly699, interprets these data in terms of the probe-binding cleft conformation during hydrolysis. The visible wavelength induced CD from 5′IAF modified Cys707 in S1 at the absorption band of the fluorescein provides an additional structural signal that is also interpreted in terms of the probe-binding cleft conformation during hydrolysis using model calculations.

The data from time-resolved fluorescence intensity changes following length transients in fibers and from the CD signals from extrinsic and intrinsic probes within the probe-binding cleft combine to form a consistent picture for the probe-binding cleft conformation during hydrolysis with the use of a Gly699 pivot as a model for the myosin structural changes accompanying hydrolysis.

MATERIALS AND METHODS

Chemicals. The fluorescent labels, 5′-iodoacetamidofluorescein (5′IAF) and 5′-iodoacetamidotetramethylrhodamine (5′IATR), are from Molecular Probes (Eugene, OR). ADP, ATP, dithiothreitol (DTT), α-chymotrypsin, 5,5′-dithiobis-(2-nitrobenzoate) (DTNB), dimethyl(2-hydroxy-5-nitrobenzyl)sulfonium bromide (DHNBS), Triton X100, creatine kinase, phosphocreatine, and phenylmethanesulfonyl fluoride (PMSF) are from Sigma Chemical (St. Louis, MO). All chemicals are analytical grade.

Solutions. Rigor solution contains 80 mM potassium chloride, 5 mM magnesium chloride, 2 mM ethylene glycol bis(β-aminoethyl ether)-*N*,*N*,*N*′,*N*′-tetraacetic acid (EGTA), 1 mM DTT, 0.2 mM PMSF, and 5 mM phosphate buffer. Relaxing solution is rigor solution plus 4 mM ATP. MgADP solution is rigor solution plus 4 mM ADP. Activating solution is relaxing solution with 0.1 mM $CaCl_2$ replacing the EGTA. Glycerinating solution is relaxing solution plus 50% glycerol (volume-to-volume). Skinning solution is relaxing solution plus 0.5% Triton X100. Labeling solution is relaxing solution without DTT. All solutions are pH 7.0.

Preparation and Modification of Myosin Subfragment 1. Rabbit myosin was prepared by a standard method (*19*) and S1 by digesting myosin filaments with α-chymotrypsin (*20*). S1 (10−25 μM) was modified in 25 mM TES plus 0.2 mM PMSF at pH 7.0 for 12 h at 4 °C with a 1.2-fold molar excess of 5′IAF. Excess dye was removed by gel filtration (Sephadex Column, BioRad 10DG) into rigor buffer then exhaustive dialysis. This procedure produced fluorescein labeled S1 (5′F-S1) with 60−70% of the SH1's modified (*21*).

We also modified S1 with DHNBS as in Werber et al. (*22*). S1 (10−25 μM) was modified in 20 mM MES at pH 6.0 for 10 min at 0 °C with a 10−15-fold molar excess of DHNBS. The reaction of DHNBS with S1 was quenched by addition of 5 mM DTT. Excess DHNBS was removed by exhaustive dialysis against 20 mM Tris−HCl, 1 mM EDTA, and 150 mM KCl or NaCl, pH 7.8. The DHNBS labeled S1 (D-S1) was equilibrated with 20 mM Tris−HCl, pH 7.8 by passing it through a Sephadex Column (BioRad 10DG). The concentration of DHNBS was determined in the presence of 0.14 N NaOH (pH > 12.0) using an extinction coefficient of 18400 $(M\ cm)^{-1}$ for DHNBS. Protein concentration in D-S1 was measured by Bradford BioRad Microassy or by using absorption after correcting appropriately for the absorption of the DHNBS at 280 nm. We incorporated 0.70−0.85 DHNBS groups per S1 with this protocol.

We investigated DHNBS modification of the thiols in S1 by determining the number of free SH's in native and

modified S1 by Ellman's method (*23*). S1 and D-S1 were denatured in 8 M urea pH 8.0 and reacted with DTNB. Under our labeling conditions, the number of free thiols in S1 and D-S1 were 10.0 and 10.2, respectively, suggesting no modification of the cysteine residues by DHNBS. We observed K^+−EDTA and Ca^{2+} ATPase of D-S1 to be 89% and 117%, respectively, of the native S1. The addition of MgATP increased tryptophan fluorescence for S1 and D-S1 by 19.4% and 21.7%, respectively. These ATPase and fluorescence results are in good agreement with previously published measurements (*22, 24*).

Preparation, Modification, and Decoration of Muscle Fibers. Rabbit *psoas* muscle fibers were obtained as previously described (*25*) and kept in glycerinating solution at −15 °C for up to several weeks. Glycerinated fibers were separated into bundles containing 100−200 fibers each, washed for 10 min in relaxing solution, and then transferred to skinning solution for 30 min. Skinned fibers were washed in labeling solution for 10 min to remove Triton X100 and DTT, and then reacted with 120 μM 5′IAF or 70 μM 5′IATR in labeling solution for 30 min. The reaction was stopped with 1 mM DTT, and the excess dye was washed out with relaxing solution. All fiber treatments were conducted at 4 °C with intense stirring. Approximately 80% of the total intensity emitted from the 5′IAF or 5′IATR label in modified fibers originated from the myosin heavy chain while the remaining probe intensity was distributed among actin, myosin light chain 1, and α-actinin in agreement with earlier work (*21, 26*). There was no significant labeling of tropomyosin in the fiber by either probe.

The location of the probe on the myosin heavy chain was evaluated by comparison of the Ca^{2+} and K^+−EDTA ATPase activities of myosin extracted from labeled fibers as described earlier (*27*). The myosin K^+−EDTA ATPase activity of the 5′IAF or 5′IATR labeled myosin extracted from the fibers indicates a 0.35 or 0.32 probe/S1 molar ratio and that all of the probe on the myosin heavy chain resides on SH1 in agreement with earlier work (*21, 26*). Fibers labeled to this degree exhibited transient rigor tension indistinguishable from that produced by similarly handled but unmodified fibers. These results suggests no measurable impairment of rigor tension due to the modification of SH1 with 5′IAF or 5′IATR.

In some experiments, fiber bundles prepared for labeling were not treated with probe but otherwise handled identically, then dissected into single fibers that were mounted on the tension transducer (see below) and decorated in rigor buffer with 1−2 mg/mL 5′F-S1 for 15 min at 4 °C. Unbound 5′F-S1 was washed out from the single fibers with rigor solution.

Time-Resolved Fluorescence Measurements on Muscle Fibers. Time-resolved fluorescence intensity measurements on single glycerinated muscle fibers were carried out using the instrument and fiber handling procedures described previously (*28*). An inverted epi-illumination microscope focuses excitation light onto the fiber sample and collects emitted fluorescence, and a length/tension controller on the microscope stage applies the length transients to the fiber. The instrument is under computer control to synchronize the time-resolved observation of fluorescence with the length transient. The computer also digitizes the incoming data stream and performs signal averaging.

Single fibers of 2 mm length were mounted on the length/tension controller under rigor conditions. The fiber was relaxed, stretched slightly until passive tension was detectable, then returned to rigor conditions. Following development of maximal rigor tension the fiber was subjected to multiple stretch/release cycles. During each cycle, the time-resolved change in the polarized fluorescence intensities $I_{\parallel,\parallel}$ and $I_{\perp,\parallel}$, or $I_{\perp,\perp}$ and $I_{\parallel,\perp}$, emitted by a cross-bridge bound probe were recorded simultaneously. Subscripts $\parallel$ and $\perp$ refer to the direction of light polarization relative to the fiber symmetry axis, the first to excitation and the second to emission. Polarization intensities from a single stretch/release cycle were signal averaged over several cycles. Fiber length change rates were 3 nm per half-sarcomere per 1.5 ms. In stretch/release experiments conducted on decorated fibers, unlabeled fibers were decorated with 5′F-S1 after development of the rigor tension. Fluorescence intensity from the decorated fibers decreased immediately by more than a factor of 10^3 upon addition of relaxing solution indicating that unbound 5′F-S1 contributed little to the signal from the decorated fibers in rigor. All experiments were conducted at 4 °C.

The polarized fluorescence from the cross-bridge bound probe detects change in cross-bridge orientation. The polarization ratios $P_\parallel$, $P_\perp$, $Q_\parallel$, and $Q_\perp$ defined as

$$P_\parallel \equiv \frac{I_{\parallel,\parallel} - g_m I_{\parallel,\perp}}{I_{\parallel,\parallel} + g_m I_{\parallel,\perp}} \qquad P_\perp \equiv \frac{g_m I_{\perp,\perp} - I_{\perp,\parallel}}{g_m I_{\perp,\perp} + I_{\perp,\parallel}} \tag{1}$$

$$Q_\parallel \equiv \frac{I_{\parallel,\parallel} - g_e I_{\perp,\parallel}}{I_{\parallel,\parallel} + g_e I_{\perp,\parallel}} \qquad Q_\perp \equiv \frac{g_e I_{\perp,\perp} - I_{\parallel,\perp}}{g_e I_{\perp,\perp} + I_{\parallel,\perp}} \tag{2}$$

quantify the polarized fluorescence, where g_e and g_m correct for the polarization dependent transmission efficiency of excitation and emission light intensity through the instrument optics. Only three of the quantities $P_\parallel$, $P_\perp$, $Q_\parallel$, and $Q_\perp$ are independent, but all are listed to facilitate comparison with previous results.

Hellen et al. (*29*) computed the polarized intensities for a muscle fiber located at the origin of the lab frame coordinates with symmetry axis parallel to the *z*-axis, excitation light propagating in the $-y$-direction, and emission light collected along the $+y$-axis with a low aperture objective. There it was shown that for probe angular distribution *N*,

$$I_{\parallel,\parallel} = \alpha I_T \int N(\theta)(2\cos^2\omega\cos^4\theta + \sin^2\omega\cos^2\theta\sin^2\theta)\sin\theta\,d\theta \tag{3}$$

$$I_{\parallel,\perp} = \alpha I_T \int N(\theta)(\cos^2\omega\sin^2\theta\cos^2\theta + \sin^2\omega\cos^2\theta(1 - {}^1/_2\sin^2\theta))\sin\theta\,d\theta \tag{4}$$

$$I_{\perp,\parallel} = \alpha I_T \int N(\theta)(\cos^2\omega\sin^2\theta\cos^2\theta + {}^1/_2\sin^2\omega\sin^4\theta)\sin\theta\,d\theta \tag{5}$$

$$I_{\perp,\perp} = \alpha I_T \int N(\theta)({}^3/_4\cos^2\omega\sin^4\theta + {}^1/_2\sin^2\omega\sin^2\theta(1 - {}^3/_4\sin^2\theta))\sin\theta\,d\theta \tag{6}$$

for a probe with absorption dipole polar angle θ and emission dipole located anywhere on the surface of a cone of half-

angle ω, where ω is the angle between the absorption and emission dipoles. Constant α accounts for microscope optics collection efficiency. We use $\omega = 19°$ or 17° for 5′IAF or 5′IATR labeling cross-bridges in muscle fibers (*21*, *26*). Solving eqs 3−6 for the total fluorescence intensity emitted by a labeled fiber, I_T, we obtain

$$\alpha I_T = {}^1/_2 I_{||,||} + I_{||,\perp} + \frac{I_{\perp,||} + ({}^4/_3) I_{\perp,\perp}}{1 - {}^1/_3 \sin^2 \omega} \quad (7)$$

The normalized total intensity, $I(t)$, is $\alpha I_T(t)$ divided by the average total light intensity before the length perturbation, $\langle \alpha I_T(-) \rangle$, such that

$$I(t) = I_T(t)/\langle I_T(-) \rangle \quad (8)$$

Steady-State Tryptophan Fluorescence Measurements from S1 in Solution. All fluorescence spectra were recorded at 4 °C on a SLM 8000 spectrofluorometer (SLM instruments, Urbana, IL) with monochromator slits of 2−4 nm. Tryptophans in S1 were excited with 295 nm light and we quantitated tryptophan emission using emitted light intensity at 336 nm or using the area from the emission band integrated from 320 to 354 nm.

CD and FDCD Measurements. All CD spectra were recorded using a Jasco J720 spectropolarimeter (Jasco Inc., Tokyo, Japan) with 2 nm bandwidth excitation. FDCD spectra were recorded at 6 °C on the J720 modified as described previously (*18*). Emission from the indole of tryptophan was selected using a band-pass filter (400 ± 50 nm). FDCD spectra were signal averaged for ∼24 min.

For FDCD experiments, we prepared samples with absorption at 280 nm, $A_{280} \leq 0.05$, and recorded the optical activity, $S_{FDCD} = K(F_L - F_R)$ in mdeg, where $F_{R(L)}$ is the fluorescence emitted after excitation by right (left) circularly polarized light and K is the spectropolarimeter calibration constant. We showed previously that probe modification of SH1 by 5′IAF quenches Trp510 but leaves unchanged the emission from all of the other tryptophan residues (*8*, *18*) so that the difference in the tryptophan emission in the FDCD spectra between identical protein concentration samples of S1 and 5′IAF-S1 originates solely from Trp510 emission such that

$$\Delta S_{FDCD} \equiv S_{FDCD}(S1) - S_{FDCD}(5'F\text{-}S1) = -KCl\,[\Delta\epsilon_{510} + (\textstyle\sum_i E_i \Delta\epsilon_i)]\phi_{510} \quad (9)$$

where C is the 5′F-S1 concentration, l is the optical path length, $\Delta\epsilon_{510}$ and ϕ_{510} are the FDCD extinction coefficient and quantum efficiency of Trp510 in native S1, E_i is the efficiency of fluorescence resonance energy transfer (FRET) to Trp510 from, and $\Delta\epsilon_i$ is the FDCD extinction coefficient of the ith tyrosine residue in the neighborhood of Trp510 in native S1. We also measured fluorescence from the same sample on the fluorescence spectrometer. The difference in the tryptophan emission, ΔF, between identical protein concentration samples of S1 and 5′F-S1 also originates solely from Trp510 emission such that

$$\Delta F \equiv F(S1) - F(5'F\text{-}S1) = K'Cl\,\epsilon_{510}\phi_{510} \quad (10)$$

where F is the tryptophan fluorescence intensity, K' is the fluorometer calibration constant, and ϵ_{510} is the extinction coefficient of native Trp510. Equation 10 does not include a contribution from tyrosine since we excite fluorescence at 295 nm where tyrosine does not absorb. After integrating eq 9 over wavelength, we form the ratio of eqs 9 and 10 to eliminate the quantum efficiency such that

$$\frac{\int \Delta S_{FDCD}\, d\lambda/\lambda}{\Delta F} = \frac{-K''[R_{510} + (\sum_i E_i R_i)]}{D_{510}} \quad (11)$$

where K'' is a new proportionality constant, dipole strength $D_{510} \propto \epsilon_{510}$, and the rotary strength $R_{510} + \sum_i E_i R_i \propto \int(\Delta\epsilon_{510} + \sum_i \Delta\epsilon_i E_i)\, d\lambda/\lambda$ (*30*). We also use a ratio of signals from Trp510 in the presence/absence (±) of nucleotide or nucleotide analog to obtain the dimensionless relative optical activity, S, defined by

$$S \equiv \frac{\Delta F(-)}{\Delta F(+)} \frac{\int \Delta S_{FDCD}\,(+)\, d\lambda/\lambda}{\int \Delta S_{FDCD}\,(-)\, d\lambda/\lambda} = \frac{D_{510}\,(-)}{D_{510}\,(+)} \frac{R_{510}\,(+) + \sum_i E_i R_i\,(+)}{R_{510}\,(-) + \sum_i E_i R_i\,(-)} \quad (12)$$

The middle expression of eq 12 contains the observable quantities. The expression on the right side of eq 12, calculable from the conformation of the peptide in the vicinity of Trp510, is an intrinsic characteristic of the S1 structure.

Calculation of the Optical Signal. The peak absorption energy, and, dipole and rotary strengths for electronic transitions contributing to the near-UV tryptophan CD and FDCD signals were calculated as described previously (*18*) but including more interactions among the S1 residues. The calculation combines the two observable lowest energy transitions of the peptide amide group, the (n,π^*) and (π,π^*) transitions, with the observable (π,π^*) transitions from aromatic side chains or fluorescein modifying Cys707. The Coulomb potential with vacuum dielectric constant couples the transition monopoles of these excited states from interacting groups. The aromatic side chains considered include tryptophan, tyrosine, phenylalanine, and histidine. The position and value of the transition monopole charges for the peptide amide group (*31*) and the aforementioned side chain groups (*32*−*35*) were taken from the literature.

Bond lengths and angles for fluorescein were taken from the crystal structure of disodium fluorescein (*36*) and used in the semiempirical quantum mechanical method ZINDO/S with configuration interaction (CI) (*37*) to calculate the electric dipole orientations and strengths for the visible part of the absorption spectrum. Calculations were carried out on the deprotonated molecule in a vacuum with a charge of −2 and zero electronic spin in the ground state. The nearly perpendicular relative orientation of the planes containing the xanthene and benzene groups in the crystal structure was adjusted slightly to improve agreement between the calculated and observed dipole moment orientations (*38*) and transition energies for the lowest allowed electronic transitions for fluorescein in buffer at pH 7 where the molecule is deprotonated (*39*). The energy penalty for this structure adjustment was within a 10−15 kcal/mol energy barrier (i.e.,

Table 1: Calculated Atomic Charges for Fluorescein[a]

atom	ground state	transition 1[b]	transition 2[c]
C1	+0.0045	−0.0104	−0.0277
C2	−0.2264	−0.0430	−0.1179
C3	−0.3224	+0.0203	−0.0278
C4	−0.0728	+0.0046	−0.1012
C5	+0.2306	+0.0390	+0.1210
C6	+0.5199	−0.0719	−0.0693
C7	−0.0343	−0.1241	+0.1574
C8	−0.2510	−0.0638	−0.0207
C9	+1.1151	−0.2088	+0.0973
C10	−0.2460	+0.0178	−0.0558
C11	−0.1522	+0.0127	+0.0138
C12	+0.7913	−0.2862	−0.4308
C13	−0.1223	+0.2758	+0.0960
C14	+0.3339	+0.1284	+0.0750
C15	−0.3014	+0.0909	+0.0186
C16	+1.4590	+0.1649	+0.0355
C17	−0.4564	+0.1263	+0.0122
C18	+0.8528	+0.1344	−0.0266
O19	−1.3400	−0.0348	−0.0397
O20	−4.0086	−0.3007	+0.3041
O28	−3.4380	+0.3921	+0.1664
C30	+0.8385	−0.2440	−0.0259
C31	+2.3224	−0.0026	−0.0075
O32	−3.3105	−0.0124	−0.0366
O33	−3.7857	−0.0045	−0.1098

[a] Atom numbering from Figure 1. All charges in units of 10^{-10} esu where the electron charge is −4.8. The total charge in the ground state is −9.6 and transition monopole charges sum to 0. The monopoles for transitions $i = 1, 2$ are equivalent to dipole vectors $\mathbf{D}_i = |\mathbf{D}_i|(\sin\theta_i \cos\phi_i, \sin\theta_i \sin\phi_i, \cos\theta_i)$ where $|\mathbf{D}_{1,2}|^2 = 43.9, 9.4$ debye^2; $\theta_{1,2} = 6°, 111°$; $\phi_{1,2} = 280°, 276°$; the molecular frame z-axis is parallel to the long axis of the xanthene ring, and the y-axis is in the plane of the xanthene and pointing toward the benzoyl group. The calculated dipole orientations mimic those observed from probes with similar structure and spectroscopic properties (*38*). [b] Calculated transition wavelength maximum of 478 nm compares with the observed value of 494 nm. [c] Calculated transition wavelength maximum of 348 nm compares with the observed value of 336 nm.

about half the average energy fluctuation of fluorescein at 4 °C). We computed the net transition monopole charge at each atom in the molecule from the electron density matrix generated in ZINDO/S as described elsewhere (*11*). The amplitudes of the transition monopoles were normalized to reproduce the observed dipole strengths of fluorescein.

Monopole charge on carbon or oxygen atoms in the benzene and xanthene rings of fluorescein were split into two equal point charges and placed equidistant from the atom along a line perpendicular to the plane of the ring in the region of the π-orbital. We used the separation distance between a carbon or oxygen atom and its monopole charge suggested by Bayley et al. (*31*). Monopole charge from hydrogen atoms were summed with those from the nearest ring carbon and monopole charges from the COO^- group were placed at the atomic coordinate. Table 1 summarizes the results of the transition monopole calculation for fluorescein for the atom numbering given in Figure 1.

Experiment and calculation are compared for energy, dipole strength, and rotary strength at the two lowest energy transitions of tryptophan, assigned ^1L_b and ^1L_a, and having unperturbed mean absorption at 294 and 284 nm (*34*), and the lowest energy transition of tyrosine, assigned ^1L_b, and having the unperturbed mean absorption at 275 nm (*33*). We assume complete overlap of the tryptophan ^1L_a and tyrosine ^1L_b transition bands such that when both contribute to a

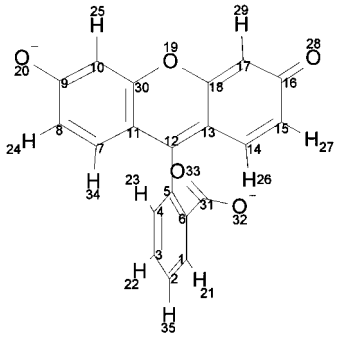

FIGURE 1: The fluorescein molecule used in the calculation of transition monopoles given in Table 1 with the numbering of atoms indicated.

spectrum their contributions are summed. When appropriate, experiment and calculation are also compared for fluorescein at its two lowest energy transitions having unperturbed mean energies of 494 and 336 nm (*15*).

The vacuum Coulomb potential accurately models the interaction between charges separated by nonpolarizable matter. In a protein, the transition monopoles separated by more than a few angstroms must interact less strongly due to the polarizability of the surrounding atoms. We account for this "charge screening" effect, as have others (*16*, *17*), by confining interactions among monopoles to those within the neighborhood surrounding the tryptophan, tyrosine, or fluorescein modified cysteine target residue. Limiting monopole interactions also keeps the numerical problem tractable since considering all of the interactions possible in chymotryptic rabbit S1 with 5 tryptophans, 35 tyrosines, 49 phenylalanines, 18 histidines, plus the backbone interactions is beyond our computer hardware capabilities. For a given target residue, we considered interactions among the amide groups within 8 Å and other aromatic side chains within 14 Å of the target C_γ carbon. The longer cutoff for the aromatic side chain interactions compensates for the smaller difference in transition energies between a target and other aromatic residues giving the latter the potential to significantly perturb observable quantities of the target from larger distances. We show below that these interaction distance cutoffs lead to reliable predictions for rotary strengths from S1 and Trp131.

We use results from CD and FDCD, two approaches for measuring the optical activity of chiral molecules, that are not necessarily equivalent. S1 in solution does not dynamically depolarize tryptophan emission following excitation by circularly polarized light so that FDCD from S1 exhibits the effect of photoselection (*40*). In the past we calculated the effect of photoselection and interpreted the uncorrected FDCD derived extinction coefficient, rather than altering the experimental setup to remove the effect of photoselection from the observed FDCD signal (*18*). We continue this approach here with care taken to distinguish the two kinds of extinction coefficients or rotary strengths by referring to those containing the effect of photoselection as FDCD extinction coefficients or FDCD rotary strengths.

Comparison of Rabbit and Chicken S1 Sequences. We use the chicken S1 sequence numeration of Maita et al. (*41*) and the crystallographic structure of chicken S1 with coordinates obtained from the Brookhaven Protein Data Bank (2mys) (*6*). While both chymotryptic rabbit and chicken S1 contain just 5 tryptophan residues (M. C. Schaub and R. A.

Zuellig, Institute of Pharmacology, University of Zurich, Zurich, Switzerland, personal communication), several residues in their sequences differ (*42*). The impact of these changes on calculated signals is discussed when appropriate in the Results.

Computer Generated Structure Changes in S1. X-ray crystallography provides the atomic coordinates for S1 needed to calculate the optical signal. We modified the Ramachandran angles of Gly699 (ϕ_{699},ψ_{699}), generating structural models of S1 that imitate changes during energy transduction to estimate the accompanying changes in the optical signal. The crystallographic structure of chicken S1 has (ϕ_{699},ψ_{699}) = (118.3°,−13.7°). Varying ϕ_{699} and/or ψ_{699} and rotating residues between Val700 and the C-terminus as if they made up a rigid body generated the new structures. Changes in (ϕ_{699},ψ_{699}) from (118.3°,−13.7°) cause atomic clashes when atoms not covalently bound (nonbonded atoms) approach each other at distances ≤ 2 Å. We best avoided clashes in our model system by holding ϕ_{699} constant and equal to 118.3° while allowing ψ_{699} to vary. In the domain $-50° \leq \psi_{699} \leq 50°$, S1 undergoes structural change causing displacement of the C-terminus at the tip of the lever arm of S1 by ∼100 Å. Varying ψ_{699} such that $-50° \leq \psi_{699} \leq -13.7°$ causes nonbonded atoms to clash from the heavy chain atoms in residues 32−35 or 95−99 with various residues numbering ≥ 702. Consequently, adaptation of these model S1 structures to a minimum energy configuration could possibly involve only local and minimal structural rearrangement in residues 32−35, 95−99, and/or in residues numbering ≥ 702. Varying ψ_{699} such that $0° \leq \psi_{699} \leq 50°$ causes more numerous clashes throughout S1 suggesting the corresponding minimum energy configuration would likely involve more widespread structural rearrangement in S1. The $0° \leq \psi_{699} \leq 50°$ domain is also sterically forbidden for a glycine residue in a polypeptide chain (*43*, *44*).

Curve Fitting. We fitted absorption and CD spectra to estimate dipole and rotary strengths. Gaussian shaped absorption bands were assumed in all cases. A least-squares protocol with equality and inequality constraints (*45*) located the best fitting linear parameters (amplitudes). The best nonlinear parameters (spectral maxima and widths) were located by grid search.

RESULTS

Effect of Length Transients on Fluorescein Fluorescence in Muscle Fibers. Figure 2 shows the time course of normalized fluorescence intensity *I*, force per unit area *F/A*, and length *L*, for 5′IAF and 5′IATR labeled fibers, as well as for an unlabeled fiber decorated with 5′F-S1. Also shown is the time course of $Q_{||}$ for a 5′IAF labeled fiber in rigor. Comparison of *I*(*t*) for 5′IAF labeled fibers in rigor (●) and relaxation (□) show that the light intensity decreases 5.0 and 0.5%, respectively, when length increases. The decrease in relaxation is statistically insignificant while the significant decrease in rigor suggests a strain induced decrease in probe quantum efficiency. Comparison of *I*(*t*) from 5′IAF (●) and 5′IATR (○) labeled fibers in rigor indicate that the rhodamine probe has a smaller but significant strain induced decrease in probe quantum efficiency. The difference between 5′IATR and 5′IAF labeled fibers in response to cross-bridge strain is expected on the basis of previous results where these

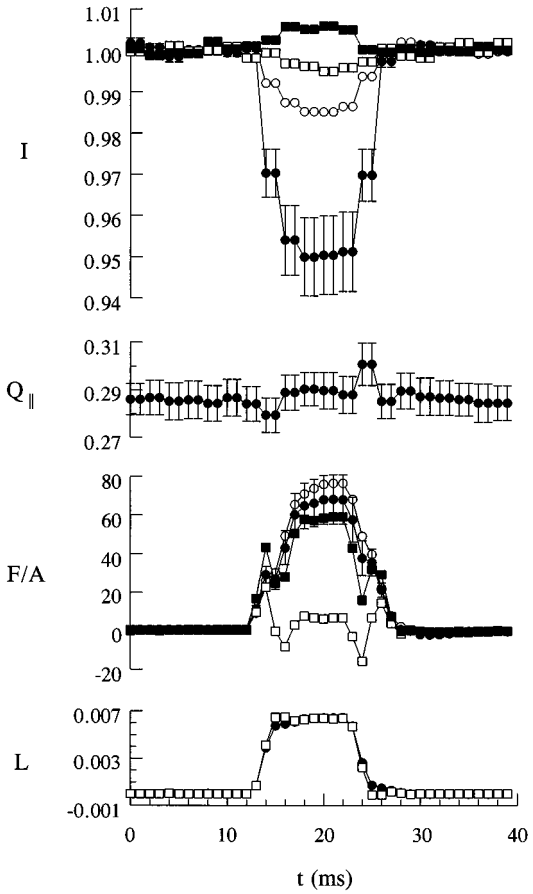

FIGURE 2: The normalized total intensity *I*, the polarization ratio $Q_{||}$, force per unit area *F/A* in kN/m^2, and transient displacement *L* in millimeters, from 2 mm long muscle fibers. Fibers were subjected to transients of 0.3% of the total fiber length that first stretched the fiber then returned it to its original length. Shown are average traces from 5′IAF labeled fibers in rigor (●) or relaxation (□), 5′F-S1 decorating unlabeled fibers in rigor (■), and 5′IATR labeled fibers in rigor (○). Each trace combines data from several fiber preparations. Vertical bars show standard error for 5′IAF labeled fibers in rigor and are typical of the other curves in each panel. The *F/A* curves show an instability during the length transient that was contributed by the tension transducer. The *L* curves, showing only 5′IAF labeled fibers, are identical to curves from unlabeled or 5′IATR labeled fibers. Time resolution is 2 ms.

probes modifying SH1 in S1 react quite differently to nucleotide and/or actin binding to S1 (*13*, *46*). In relaxation, emission from 5′IATR modified fibers (data not shown) behaves identically to that from 5′IAF labeled fibers during length transients. The *I*(*t*) from unlabeled fibers in rigor decorated with 5′F-S1 (■) changes insignificantly in response to the length transient suggesting that the length transient does not induce an artifactual intensity change due to the translation of the sample.

The fluorescein quantum efficiency in 5′F-S1 decreases by a factor of 4 upon 5′F-S1 detachment from actin (*13*) suggesting strain induced cross-bridge detachment in 5′IAF labeled fibers in rigor be considered as the cause of decreasing *I*(*t*) during length transients. However, the reversibility of the change in *I*(*t*) due to the length transient and the close correlation between *I*(*t*) and *F*(*t*) over the entire time domain indicates that strain in the rigor cross-bridges is the cause of time-dependent changes in *I*(*t*) not cross-bridge detachment from actin. Comparison of force traces from 5′IAF labeled (●) and unlabeled (■) fibers in rigor

Table 2: Calculated Rotary Strengths from Tryptophans in S1[a]

angle	residues					S1
ψ_{699}	Trp113	Trp131	Trp440	Trp510	Trp595	total
−50°				+0.0306		+0.0422
				−0.057		−0.0645
−40°				+0.0376		+0.0493
				−0.0881		−0.0956
−30°				+0.0498		+0.0615
				−0.1514		−0.1589
−20°				+0.0538		+0.0655
				−0.1672		−0.1747
−13.7°				+0.0521		+0.0637
				−0.1357		−0.1432
+0°	−0.1211	+0.1182	−0.0009	+0.0515	+0.0155	+0.0631
	−0.4786	+0.5592	+0.0313	−0.1551	−0.1194	−0.1626
+10°				+0.0451		+0.0567
				−0.1806		−0.1881
+20°				+0.0399		+0.0516
				−0.1151		−0.1226
+30°				+0.0371		+0.0487
				−0.0948		−0.1022
+40°				+0.0384		+0.0500
				−0.0857		−0.0931
+50°				+0.0384		+0.0500
				−0.0857		−0.0931

[a] Rotary strengths in debye−bohr magnetons for the ^1L_b (upper value) and ^1L_a (lower value) absorption bands of tryptophan. The rotary strengths of Trp113, 131, 440, and 595 do not change as a function of ψ_{699}. The rotary strength of Trp510 is affected by changes in ψ_{699} principally because of movement between Tyr758 and the Tyr503−Trp510 complex.

indicate that modified and native fibers develop identical rigor tension showing the modified cross-bridges do not preferentially detach during the length transient further supporting the notion that strain in the 5′IAF modified cross-bridge causes the quantum efficiency change in the probe.

We observed the time dependence of the polarization ratios $P_{||}$, $P_{\perp}$, $Q_{||}$, and $Q_{\perp}$ to detect cross-bridge orientation during length transients on 5′IAF and 5′IATR labeled fibers in rigor and relaxation, as well as for unlabeled fibers in rigor decorated with 5′F-S1. In each case the orientation of the cross-bridge is insignificantly changed by the length transient in agreement with earlier results from probes of SH1 (*28, 47*). $Q_{||}$ from 5′IAF labeled fibers in rigor (●) is typical of cross-bridge response to the length transient. The time-averaged polarization ratios for 5′IAF labeled fibers in rigor or relaxation are $P_{||} = 0.27 \pm 0.02$, $P_{\perp} = 0.28 \pm 0.01$, $Q_{||} = 0.29 \pm 0.03$, and $Q_{\perp} = 0.26 \pm 0.01$ or 0.34 ± 0.01, 0.30 ± 0.02, 0.35 ± 0.01, and 0.29 ± 0.01, respectively, in agreement with earlier work (*21*). Values observed for 5′IATR labeled fibers in rigor and relaxation are identical to those reported earlier (*28, 29*).

The Near-Ultraviolet CD Spectrum of Myosin S1. Table 2 indicates the calculated rotary strengths for the indole ^1L_b and ^1L_a transitions as a function of ψ_{699} for the five tryptophan residues 113, 131, 440, 510, and 595 in rabbit chymotryptic S1. Sequence differences between chicken and rabbit S1 potentially impact the calculated rotary strengths of Trp440 and Trp595 due to the rabbit/chicken substitutions of Phe621/Leu621 and Leu475/Phe475, respectively. Trp440 is 7.0 Å from residue 621, while Trp595 is 4.6 Å from residue 475. The effect of these substitutions was easily modeled within the chicken S1 structure since both side chains contain C_β, C_γ, and two C_δ's allowing reliable positioning of either side chain in both residue positions. We found that these substitutions had no significant affect on the rotary strengths tabulated in Table 2.

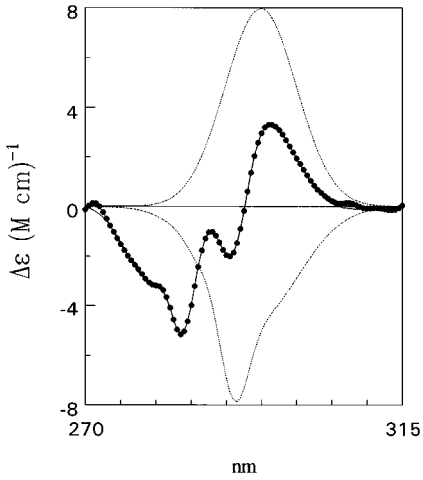

FIGURE 3: The near-UV CD extinction coefficient of S1 (●), the best fitting curve (—), and the estimates for the positive contribution from ^1L_b and negative contribution from ^1L_a (broken lines). This spectrum was obtained from S1 in 25 mM HEPES and 0.1 M KCl at room temperature and pH 7. Table 2 contains calculated rotary strength estimates appropriate for this sample.

The calculated values in Table 2 show that only the rotary strength of Trp510 varies with ψ_{699}. We found that this is due principally to a changing interaction strength among Trp510, Tyr503, and Tyr758, caused by alteration of the distance and orientation of Tyr758 relative to Trp510 and Tyr503 when pivoting at Gly699. The sum of the contributions from the residues listed in Table 2 should represent the rotary strength of tryptophan in S1 that may be compared with the values observed for this protein.

Figure 3 shows the near-UV CD spectrum of S1, obtained from S1 in 25 mM HEPES and 0.1 M KCl at room temperature and pH 7. We attributed transitions occurring with peak wavelengths, > 285 nm to the indole transitions ^1L_b and ^1L_a in the sum of Gaussian shaped absorption bands that make up the fitted curve and found energies of 294.8 and 290.8 nm and rotary strengths of +0.067 and −0.061 D−B (debye−bohr magneton), respectively. The peak energy of the ^1L_a transition is higher than that usually suggested for this transition (*18, 32*) possibly due to the inadequacy of one or two Gaussian bands to accurately represent the complicated shapes of the ^1L_b and ^1L_a transitions (*48*) and because the contributions from tryptophan and tyrosine are not separable in the wavelength region occupied by tryptophan ^1L_a. Nevertheless, the fitted curve gave no indication of a positive amplitude band for wavelengths ≥ 270 nm, except for the lowest energy band that is certainly tryptophan ^1L_b, and strongly supports the assignment of negative amplitude rotary strength to tryptophan ^1L_a. These observed values are comparable with all of the total calculated S1 signals listed in Table 2 and do not suggest a preferred value for ψ_{699}.

The Near-Ultraviolet FDCD Spectrum of Trp131 in S1. We isolate Trp131 fluorescence from total S1 fluorescence using DHNBS modification of S1. DHNBS specifically modifies Trp131 and by taking the difference fluorescence signal between S1 and D-S1 we isolate Trp131 fluorescence, provided the modification does not affect fluorescence from the other tryptophan residues in S1. This appears to be a

Table 3: FDCD Rotary Strengths for Selected Residues and Parameters Needed to Calculate the FDCD Rotary Strength of Trp131[a]

residue	$R_{i\rightarrow113}$	$R_{i\rightarrow131}$	Δ113	Δ131	$E_{i\rightarrow113}$ (131)	$E_{i\rightarrow131}$ (113)	$E_{i\rightarrow113}$ (−)
Tyr16	+0.13	+0.03	6.1	9.9	0.94	0.05	0.99
Tyr110	−0.41	−0.40	6.6	15.5	0.98	0.01	0.99
Trp113	−0.14[b]		0	11.4	1	0	1
	−0.45[b]						
Tyr116	+0.14	+0.15	11.6	14.3	0.62	0.18	0.76
Tyr129	−0.20	−0.20	10.4	11.7	0.60	0.30	0.85
Trp131		+0.13[b]	11.4	0	0	1	0
		+0.55[b]					
Tyr135	−0.26	−0.27	13.7	7.9	0.04	0.93	0.53
Tyr195	+0.09	+0.08	22.2	17.7	0.05	0.19	0.06

[a] For tyrosine residues, $R_{i\rightarrow113}$ or $R_{i\rightarrow131}$ is the FDCD rotary strength for the ^1L_b transition of the *i*th tyrosine (i.e., Tyr16 through Tyr195 listed in the table) when Trp113 or Trp131 is the acceptor. For Trp113, the two values for $R_{113\rightarrow113}$ (designated R_{113} in the text) are the rotary strengths for the two lowest energy transitions (tryptophan ^1L_b and ^1L_a). $R_{131\rightarrow131}$ (designated R_{131} in the text) is similarly defined. All rotary strengths are in D−B. Δ113 or Δ131 is the distance in angstroms from the C_γ of Trp113 or Trp131 to the C_γ of the residue listed in the left most column. $E_{i\rightarrow113}$(131) is the energy transfer efficiency for the *i*th donor with Trp113 as acceptor while in the presence of Trp131. $E_{i\rightarrow131}$(113) is similarly defined. $E_{i\rightarrow113}(-)$ is as for $E_{i\rightarrow113}$(131) but in the absence of Trp131. [b] These values differ from the CD rotary strengths listed in Table 2 because the FDCD values contain a correction for photoselection (*40*).

reasonable supposition since key determinants of protein function including: the actin-activated, Ca^{2+}, K^+−EDTA ATPases, and the enhancement of tryptophan emission when ATP binds to S1 (*22, 24*), are minimally perturbed by modification of Trp131.

Table 3 indicates calculated FDCD rotary strengths for Trp131 and for the six tyrosine residues within or near the characteristic tyrosine−tryptophan fluorescence resonance energy transfer distance, $R_0 \approx 14$ Å, of Trp131. These tyrosine residues contribute to the FDCD signal from Trp131 by acting as donors of energy to the Trp131 acceptor and/or by interacting via the Coulomb potential. Trp113, in the vicinity of Trp131, is a competitive acceptor for these tyrosine residues so that its presence must also be accounted for in the calculation of Trp131 FDCD signal. The sequence differences between chicken and rabbit S1 do not impact the rotary strengths tabulated in Table 3.

In the native protein, FDCD from Trp131 and Trp113 comes directly from these residues and indirectly by transfer of energy from the tyrosines listed in Table 3 such that

$$-\int \Delta S_{\mathrm{FDCD}}(\mathrm{S1})\, \mathrm{d}\lambda/\lambda \propto \phi_{113} \sum_i E_{i\rightarrow113}(131) R_{i\rightarrow113} + \phi_{131} \sum_i E_{i\rightarrow131}(113) R_{i\rightarrow131} + \phi R(\text{other Trps}) \quad (13)$$

where the sum in *i* is over the six tyrosine and two tryptophan residues listed in Table 3, $R_{i\rightarrow113}$ or $R_{i\rightarrow131}$ is the FDCD rotary strength when energy transfer occurs from the *i*th residue to Trp113 or Trp131, $E_{i\rightarrow113}$(131) is the energy transfer efficiency from the *i*th residue to Trp113 in the presence of Trp131, $E_{i\rightarrow131}$(113) is analogously defined, and ϕ is the quantum efficiency.

In D-S1 the indole ring of Trp131 is modified by DHNBS implying that it will not fluoresce and that it will not readily accept energy from tyrosine via FRET because its absorbance band no longer overlaps with tyrosine emission. Then

$$-\int S_{\mathrm{FDCD}}(\mathrm{D\text{-}S1})\, \mathrm{d}\lambda/\lambda \propto \phi_{113} \sum_i E_{i\rightarrow113}(-) R_{i\rightarrow113} + \phi R(\text{other Trps}) \quad (14)$$

where $E_{i\rightarrow113}(-)$ is the energy transfer efficiency from the *i*th residue to Trp113 in the absence of a competing acceptor. Taking the difference between eqs 13 and 14 and forming the ratio equivalent to that in eq 11 gives

$$\frac{-\int \Delta S_{\mathrm{FDCD}} \mathrm{d}\lambda/\lambda}{\Delta F} = \frac{K''\{\sum_i E_{i\rightarrow131}(113) R_{i\rightarrow131} + (\phi_{113}/\phi_{131}) \sum_i [E^i_{113}(131) - E^i_{113}(-)] R_{i\rightarrow113}\}}{D_{131}} \quad (15)$$

If modification of Trp131 quenched its fluorescence but did not also change its absorption spectrum, the term with the ratio of quantum efficiencies would be zero and eq 15 would be identical to eq 11 with Trp131 replacing Trp510. We rewrite eq 15 by substituting from Table 3 for the tyrosine FDCD rotary strengths and energy transfer efficiencies to obtain

$$\frac{-\int \Delta S_{\mathrm{FDCD}} \mathrm{d}\lambda/\lambda}{\Delta F} = \frac{K''\{R_{131} - 0.2769(\mathrm{D-B}) + (\phi_{113}/\phi_{131}) 0.1568(\mathrm{D-B})\}}{D_{131}} \quad (16)$$

indicating that contributions to the FDCD signal of Trp131 from tyrosine residues tend to cancel. The calculated FDCD rotary strength from Trp131 in the tryptophan ^1L_b and ^1L_a absorption bands are $R_{131}(^1L_b) = +0.1343$ and $R_{131}(^1L_a) = +0.5545$ D−B (see Table 3). The contribution from the tyrosine in eq 16 appears in the wavelength region of $R_{131}(^1L_a)$. Given the preceding, the right-hand side of eq 16 predicts a positive near UV FDCD spectrum for Trp131, even when $\phi_{113} = 0$.

Figure 4 shows the observed near UV FDCD spectrum of Trp131. This spectrum, obtained from S1 and D-S1 in 20 mM Tris−HCl at 6 °C and pH 7.8, is equivalent with the left-hand side of eq 16 before integration over wavelength. The observed spectrum indicates a positive near UV FDCD spectrum for Trp131, in agreement with the calculation.

The Near-Ultraviolet FDCD Spectrum of Trp510 in S1. Calculation shows that Trp510 senses the global conformation of the S1 by characteristically altering its rotary strength with changing ψ_{699} (see Table 2). We have observed the FDCD spectrum from Trp510 to be sensitive to the binding of nucleotide or nucleotide analogs to the active site of S1 (*18, 49, 50*). These observations suggest comparing changes in the calculated Trp510 FDCD signal from pivoting the S1 structure at Gly699, with changes in the observed FDCD from Trp510 caused by substrate binding to the active site of S1, to assess Gly699 involvement in the energy transduction mechanism.

We computed the FDCD signal from Trp510 for S1 structures generated by altering ψ_{699}. The calculations show that interactions, via the Coulomb potential and FRET, among the three aromatic residues, Tyr503, Trp510, and Tyr758, are mainly responsible for the influence of ψ_{699} on

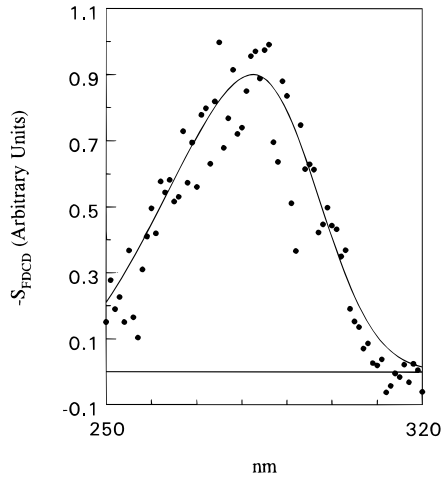

FIGURE 4: The near-UV FDCD spectrum from Trp131 (●) and the best fitting curve (—). This spectrum was obtained from S1 and D-S1 samples in 20 mM Tris−HCl at 6 °C and pH 7.8.

the near-UV FDCD signal of Trp510. Geometrically, the Tyr503−Trp510 complex is unaffected, while Tyr758 changes its distance and orientation relative to this complex, by action of the Gly699 pivot. These observations are put into quantitative form by using eq 11 where it is shown that the near-UV FDCD signal from Trp510 depends on R_{510}, the FDCD rotary strength of Trp510, and on a sum over residues Tyr503 and Tyr758 of the product of their energy transfer efficiency to Trp510 with their FDCD rotary strength. Tyr503 is within 5 Å of Trp510, so transfer efficiency is 1. Tyr758 is closest to Trp510 in the original S1 structure where $\psi_{699} = -13.7°$ but becomes more distant as ψ_{699} deviates from this value in either direction. The sequence differences between chicken and rabbit S1 do not impact the FDCD rotary strengths computed for Trp510.

Figure 5 summarizes these contributing elements to the total FDCD rotary strength of Trp510, as a function of ψ_{699} or lever arm displacement. The Trp510 FDCD rotary strengths $R_{510}(^1L_b)$ (●) and $R_{510}(^1L_a)$ (○) have opposite signs over the entire range of ψ_{699} investigated. The lowest energy tyrosine band (tyrosine ^1L_b) from Tyr503 (□) is large and positive over the entire range of ψ_{699} investigated. The lowest energy tyrosine band from Tyr758 multiplied by its energy transfer efficiency to Trp510 (△) contributes very little rotary strength, and its impact on the calculated signal is significant only through Coulomb potential interactions with Tyr503 and Trp510. Figure 5 also shows dipole strength, D_{510}, of the ^1L_b transition in Trp510 (◆) needed to compute the relative optical activity in eq 12.

$R_{510}(^1L_b)$ (●) appears in the observed FDCD spectrum of Trp510 as the lowest energy transition band. $R_{510}(^1L_a)$ (○), the lowest energy tyrosine band from Tyr503 (□), and the small contribution from Tyr758 (△) overlap in the observed FDCD spectrum and appear as the second lowest energy transition band. Their contributions are summed (■). The total observed FDCD rotary strength detected from Trp510 is the sum of the first and second transition bands (▲).

The observed Trp510 FDCD spectrum and rotary strength as a function of bound substrate to the active site of S1, reported previously (*18*), shows clearly positive amplitudes for the two lowest energy absorption bands under all conditions investigated. Comparison of this result with the

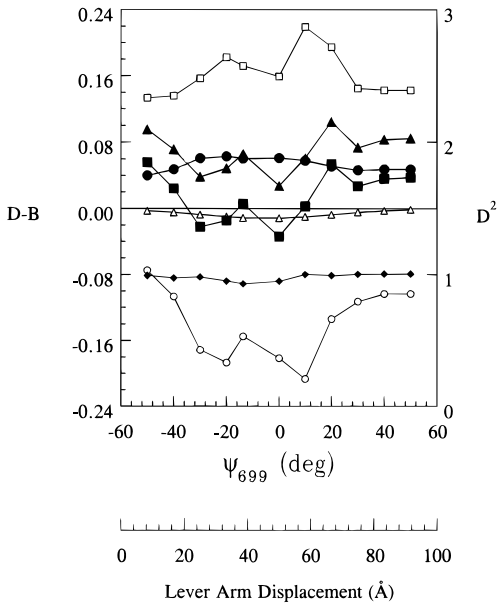

FIGURE 5: The FDCD rotary strengths in debye-bohr magnetons (D−B, left *y*-axis) of Trp510, Tyr503, and Tyr758 for emission by Trp510, and, the dipole strength of Trp510 in debye^2 (D^2, right *y*-axis) all as functions of ψ_{699} in degrees or of the C-terminus displacement in Angstroms. Shown are the FDCD rotary strengths for the Trp510 ^1L_b (●) and ^1L_a (○) transitions, the Tyr503 ^1L_b transition (□), the Tyr758 ^1L_b transition multiplied by the efficiency for energy transfer to Trp510 (△), and the dipole strength of the ^1L_b transition of Trp510 (◆). The solid lines joining the symbols are for clarity only. The Trp ^1L_a and Tyr ^1L_b FDCD rotary strengths are summed (because they overlap in the FDCD spectrum) to give the FDCD rotary strength for the observable transition with the next to lowest energy (■). The FDCD rotary strength for the observable transition with lowest energy is from Trp ^1L_b (●). The total FDCD rotary strength (▲) is the sum of the FDCD rotary strengths for the observable transitions with the two lowest energies.

Table 4: Observed Relative Optical Activities of Trp510 in the Presence of Nucleotide or Nucleotide Analogs

analog[a]	observed S^b
ADPVi	0.62 ± 0.07
$ADPBeF_x$	0.68 ± 0.07
$ADPAlF_4^-$	0.88 ± 0.17
ADP	1.03 ± 0.09
ATPγS	0.49 ± 0.18

[a] γ-Phosphate analogs include vanadate (Vi), beryllium fluoride (BeF_x), and aluminum fluoride (AlF_4^-). All data taken from ref *18*. [b] Relative optical activity *S* defined in eq 13.

calculated FDCD rotary strengths in Figure 5 suggests two regions in the ψ_{699} domain that may be ruled out on the basis of the sign of the amplitude of the second lowest energy transition band (■). They include regions on either side of, but not including, the S1 crystallographic structure at $\psi_{699} = -13.7°$ (i.e., structures with $\psi_{699} = -30°$, $-20°$, and $0°$). Table 4 indicates previously observed FDCD relative optical activities (S in eq 12) for Trp510 in the presence of various nucleotides and nucleotide analogs (*18*). This parameter decreases when any nucleotide or analog binds to the active site of S1 implying certain new restrictions (discussed below) on the domain of ψ_{699} that produces suitable S1 structures to associate with the conformation of S1 in the presence and absence of substrate.

The CD Spectrum of Fluorescein in 5′F-S1. Figure 6 has CD spectra from 5′F-S1, obtained from S1 in 50 mM TES

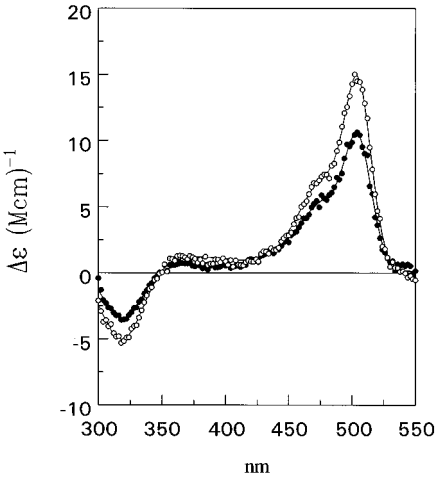

FIGURE 6: The CD extinction coefficient spectrum of 5′F-S1 obtained in 50 mM TES at room temperature and pH 7 in the absence (●) and presence of MgATP (○). The solid lines are best fitting curves. MgATP containing samples had in addition to buffer and S1, 2 mM $MgCl_2$, 1 mM ATP, and an ATP-regenerating system consisting of 0.05 mg/mL creatine kinase and 5.3 mM phosphocreatine to keep the ATP concentration constant. The rotary strengths for these spectra are tabulated in Table 5.

Table 5: Spectroscopic Characterization of 5′F-S1[a]

	wavelength		dipole strength		rotary strength	
transition[b]	1	2	1	2	1	2
$\psi_{699} = -50°$	497	337	41	8.6	0.23	−0.08
$\psi_{699} = -40°$	497	337	41	8.6	0.34	−0.14
$\psi_{699} = -13.7°$	498	338	40	7.4	0.37	−0.16
5′F-S1	502	350	40	11	0.25	−0.08
MgATP+5′F-S1	502	350	40	11	0.35	−0.14

[a] Wavelengths given in nanometers, dipole strengths in debye^2, and rotary strengths in debye−bohr magneton. Spectroscopic parameter values for $\psi_{699} = -50$, $-40°$, and $-13.7°$ are calculated; those for 5′F-S1 and MgATP+5′F-S1 are observed. [b] Transitions correspond to the lowest (1) and next to lowest (2) energy electronic transitions in fluorescein.

at 25 °C and pH 7, in the presence and absence of MgATP showing an enhancement of signal strength due to nucleotide binding. MgATP containing samples had in addition to buffer and S1, 2 mM $MgCl_2$, 1 mM ATP, and an ATP-regenerating system consisting of 0.05 mg/mL creatine kinase and 5.3 mM phosphocreatine to keep the ATP concentration constant. We showed previously that the optical activity induced in the absorption band of the fluorescein bound to SH1 in S1 is due to the close and specific interaction of the fluorescein chromophore with Trp510 (*15, 51*). Inspection of S1 structures generated by varying ψ_{699} show that a close interaction of 5′IAF bound at SH1 with Trp510 is geometrically impossible for $\psi_{699} \geq 10°$. The remaining viable structures, including $\psi_{699} = -50°$, $-40°$, and $-13.7°$, are all capable of making a suitable interaction between SH1 bound 5′IAF and Trp510. This is shown in Table 5 where we compare calculated peak energy, dipole, and rotary strengths for the two lowest energy transitions of fluorescein in 5′F-S1 for $\psi_{699} = -50°$, $-40°$, and $-13.7°$ with values observed for 5′F-S1 in the absence and presence of MgATP. These data are consistent with the association of the $\psi_{699} = -50°$ with the 5′F-S1 structure without nucleotide and larger ψ_{699} ($-40°$ or $-13.7°$) with the nucleotide bound 5′F-S1 structure. The sequence differences between chicken and rabbit S1 do not impact the calculated rotary strengths in Table 5.

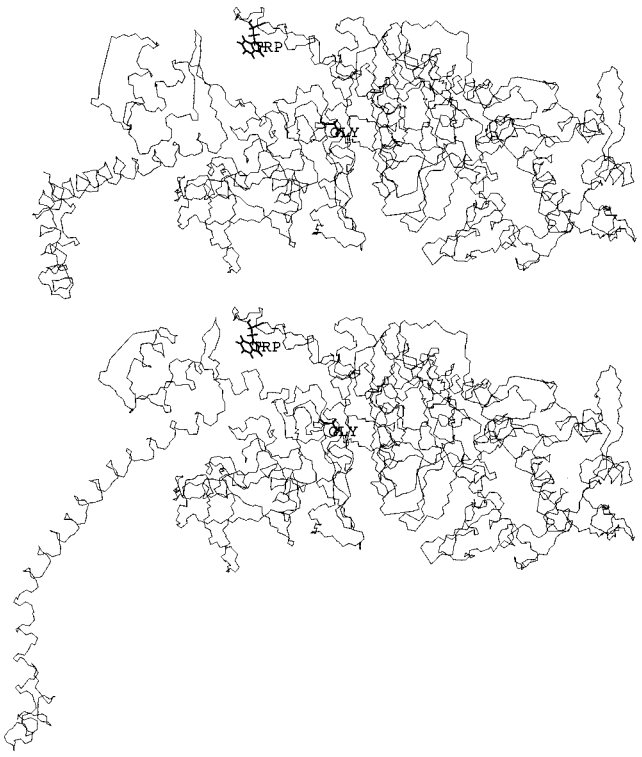

FIGURE 7: The closing of the probe-binding cleft around Trp510. The crystallographic structure of S1 with $\psi_{699} = -13.7°$ showing the peptide backbone and highlighting the Trp510 and Gly699 residues (bottom). The same structure except for $\psi_{699} = -50°$ (top), where residue 700 and higher are pivoted as in a rigid body, shows a more open conformation around Trp510. The two structures are viewed from identical aspects with respect to residues from the N-terminus through Gly699.

Our earlier work on the effect of nucleotide or nucleotide analog binding to S1 on the conformation of the probe-binding cleft gives further guidance for assigning the three candidate structures $\psi_{699} = -50°$, $-40°$, and $-13.7°$ to steps in energy transduction. We showed that the probe-binding cleft progressively closes during ATP hydrolysis by demonstrating diminished availability of Trp510 to collisional quenching as the S1 active site is occupied by nucleotide analogs that mimic successive steps in the ATPase cycle (*8*). Figure 7, showing the S1 structure in the vicinity of Trp510 for $\psi_{699} = -50°$ (top) and $-13.7°$ (bottom), demonstrates qualitatively the closing of the probe-binding cleft as ψ_{699} goes from $-50°$ to $-13.7°$. The probe-binding cleft structure for $\psi_{699} = -40°$ is intermediate to those in Figure 7. More quantitatively, C_α's from eight residues on the peptide opposite Trp510 in the probe-binding cleft lie within 10.5 Å of the Trp510−C_γ in the $\psi_{699} = -13.7°$ structure, while one residue from this peptide is within the same radius for $\psi_{699} = -50°$.

The $\psi_{699} = -50°$ structure has an open probe-binding cleft conformation suggesting it is akin to the S1 conformation without nucleotide. The more closed probe-binding cleft conformation of the $\psi_{699} = -13.7°$ structure suggests it mimics S1 with active site trapped by MgADPVi or $ADPAlF_4^-$. Given these suggestions for S1 structures during steps in the ATPase cycle, we estimate the relative optical activity expected for nucleotide analog trapped S1 based on

the data in Figure 5. We calculate S = 0.73, a value that falls within the error estimate for *S* values observed for MgADPBeF$_x$, MgADPVi, and ADPAlF$_4^-$, given in Table 4.

DISCUSSION

The end of the myosin cross-bridge ATPase cycle, following the delivery of impulsive force to the actin filament, is frequently assumed to correspond to the rigor state where the cross-bridge is tightly actin bound and without nucleotide in the active site. This assumption is supported by the observation that a muscle fiber develops significant "rigor" tension, when ATP is withdrawn from a relaxed fiber at resting length. It would seem plausible to expect that the application of an external force to a fiber in rigor, particularly one exerting rigor tension, would reverse the state of the rigor cross-bridge. In the context of the rotating cross-bridge model of contraction, reversal of the rigor state would imply cross-bridge rotation. While plausible, these expectations failed to materialize in observations from orientation sensitive fluorescent probes of SH1 (*47*) suggesting that the flexible element in myosin is between the thick filament backbone and SH1. We found that while the SH1 bound probe does not rotate significantly in response to an external force it does detect a structural change in its local environment (i.e., in the probe-binding cleft) that we have quantified with the data presented in Figure 2. This data demonstrates strain induced conformational change at the probe-binding cleft in the muscle fiber and motivates the further inquiry into the role of this part of the cross-bridge in energy transduction.

We quantify changes in the structure of S1 accompanying energy transduction using certain structurally interpretable spectroscopic signals from the solubilized native or probe modified protein. Previously we studied emission from the ATP sensitive tryptophan, Trp510, and the effect of various nucleotide analogs that mimic transient states of the ATPase cycle on its collisional quenching constant (*8*). We also measured FDCD from this residue and attempted to interpret the data structurally (*18*). These data showed the probe-binding cleft closing incrementally during the splitting of ATP from its most open conformation in rigor. Here, we reported on the application of more elaborate computational methods for structural interpretation of the CD and FDCD signals from S1 and the probe-binding cleft and introduce a structural model that accounts for the observed signals and permits visualization of the structural changes accompanying energy transduction.

Optical signals detecting conformation changes in the probe-binding cleft are easy to identify but difficult to interpret structurally. Although we apply established methods for interpreting near-UV CD and FDCD from proteins, to native and probe modified S1, the number of interacting amide groups and aromatic side chains in S1 make the problem unmanageable unless they are reduced by assumption. Naturally we chose to interact only those residues most likely to influence each other based on their spatial separations and the energy difference among their absorption bands and sought to test the assumption on structures outside of the probe-binding cleft. The near-UV CD and FDCD signals from S1 and Trp131, respectively, were predicted based on the S1 crystallographic structure and on our implementation of the computational methods (including the assumption restricting contributing interactions) and found to be consistent with the experimentally observed signals. We concluded that the optical activity of the S1 and Trp131 appear to be determined principally by the included interactions and followed the same procedure when investigating the probe-binding cleft conformation during energy transduction.

The interpretation of a changing FDCD signal from Trp510 in S1 or the fluorescein CD signal in 5′F-S1, in response to substrate binding to the active site, requires a model to appropriately alter S1 structure in the probe-binding cleft. We found a suitable model by using the Gly699 pivot shown previously to be crucial in energy transduction and force production (*12, 52*). It provides a continuum of S1 structures that can be used to calculate the optical activities of Trp510 and 5′IAF modifying SH1. This model produces the appropriate alteration in the probe-binding cleft, such that it opens and closes as ψ_{699} changes over a small domain of allowed values (see Figure 7), while causing what appears to be a manageable level of very localized atomic clashes. We did not rationalize the atomic clashes by performing energy minimization calculations to check if the perturbed S1 structure relaxes to a local energy minimum while conserving the structure of the probe-binding cleft. Consequently, we consider the findings presented here as the first approximation to rationalized transient S1 structures accompanying energy transduction.

The comparison of the CD and FDCD signals observed from fluorescein in 5′F-S1 and Trp510 in S1, in the presence and absence of nucleotide or nucleotide analogs to mimic states in the ATPase cycle, with the equivalent calculated signals from S1 structures generated by altering ψ_{699} permits association of an S1 structure with a defined state in the ATPase cycle. Our findings suggest that the cleft-open state of nucleotide-free S1 is best represented by the $\psi_{699} = -50°$ structure (Figure 7, top) and that the cleft-closed state characteristic to S1 in the process of splitting ATP is best represented by the $\psi_{699} = -13.7°$ structure (Figure 7, bottom). We find the methylated S1 crystallographic structure having $\psi_{699} = -13.7°$ to be more characteristic of the nucleotide bound rather than the nucleotide-free conformation of S1. If true, this characterization of the crystallographic structure might be attributed to the extensive methylation of lysine residues of S1 prior to crystallization (*6*) and/or to the temperature-dependent equilibrium between rigor-like and bound nucleotide-like conformations in S1 without nucleotide (*53, 54*). In the former, the methylation of S1 is associated with altered ATPases and the abolishment of Trp510 sensitivity to the binding of ATP (*55*−*57*), both indicative of significant alteration of S1 structure particularly to the probe-binding cleft region. In the latter, higher temperatures favor the rigor-like conformation of S1 while lower temperatures, and perhaps the crystal, favor the nucleotide-like conformation. Previous work showing that the shape of S1 in solution is more compact in the presence of nucleotide (*58*−*61*) provides a possible reason the crystal may prefer the nucleotide-like conformation. Finally, the crystallized methylated S1 has SO_4^- in its active site, a group known competitively inhibit nucleotide binding in myosin (*62*).

The intensity change of fluorescence from 5′IAF labeled SH1 on cross-bridges assembled in muscle fibers in rigor due to a length transient confirms the importance of the probe-binding cleft in energy transduction. The observation that the probe does not also rotate raises the issue of why intensity but not orientation of the probe responds to the length transient. It seems that the torque generated in the rigor stretch is incapable of significantly rotating the lever arm of S1 in a manner that reverses the power stroke. In the context of our model of energy transduction, the induced strain causes the distance between the probe and Trp510 to change, as suggested previously to explain 5′IAF intensity changes in 5′F-S1 (*13*), but does not cause pivoting at Gly699. The lower sensitivity of 5′IATR labeled cross-bridges to strain induced conformation change caused by the length transient is likely due to a lower sensitivity of 5′IATR to static quenching by Trp510.

In summary, we observed strain dependent conformation change in the myosin probe-binding cleft from muscle fibers in rigor suggesting that the probe-binding cleft participates in structural changes in S1 accompanying energy transduction. We further characterized the transient structure of the probe-binding cleft by interpreting CD and FDCD signals originating from this region of the cross-bridge as a function of nucleotide analogs mimicking S1 structural transients during ATPase. The interpretation of these signals was aided by a structural model of energy transduction that utilizes pivoting at Gly699 to change probe-binding cleft conformation and to displace the S1 lever arm as during force generation. We concluded that the crystallographic structure of the probe-binding cleft in S1, having a Ramachandran angle of $\psi_{699} = -13.7°$, best resembles the nucleotide bound conformation in the native protein. A different structure, characterized by $\psi_{699} = -50°$, better resembles the native rigor conformation of the probe-binding cleft. Pivoting at Gly699 rotates probes at SH1 suggesting that length transients on rigor fibers do not cause pivoting at Gly699 or reverse the power stroke.

ACKNOWLEDGMENT

We thank Drs. Marcus C. Schaub and Richard A. Zuellig from the Institute of Pharmacology, University of Zurich, Zurich, Switzerland, for making available their findings on the number of tryptophans in chymotryptic S1 prior to publication.

REFERENCES

1. Huxley, H. E. (1969) *Science 164*, 1356−1366.
2. Huxley, A. F., and Simmons, R. M. (1971) *Nature 233*, 533−538.
3. Lymn, R. W., and Taylor, E. W. (1971) *Biochemistry 10*, 4617−4624.
4. Morales, M. F., and Botts, J. (1979) *Proc. Natl. Acad. Sci. U.S.A. 76*, 3857−3859.
5. Nihei, T., Mendelson, R. A., and Botts, J. (1974) *Proc. Natl. Acad. Sci. U.S.A. 71*, 274−277.
6. Rayment, I., Rypniewski, W. R., Schmidt-Base, K., Smith, R., Tomchick, D. R., Benning, M. M., Winkelmann, D. A., Wesenberg, G., and Holden, H. M. (1993) *Science 261*, 50−58.
7. Werber, M. M., Peyser, Y. M., and Muhlrad, A. (1992) *Biochemistry 31*, 7190−7197.
8. Park, S., Ajtai, K., and Burghardt, T. P. (1996) *Biochim. Biophys. Acta 1296*, 1−4.
9. Park, S., Ajtai, K., and Burghardt, T. P. (1997) *Biochemistry 36*, 3368−3372.
10. Chabre, M. (1990) *TIBS 15*, 6−10.
11. Ajtai, K., Dai, F., Park, S., Zayas, C. R., Peyser, Y. M., Muhlrad, A., and Burghardt, T. P. (1998) *Biophys. Chem.* In press.
12. Kinose, F., Wang, S. X., Kidambi, U. S., Moncman, C. L., and Winkelmann, D. A. (1996) *J. Cell Biol. 134*, 895−909.
13. Ando, T. (1984) *Biochemistry 23*, 375−381.
14. Aguirre, R., Gonsoulin, F., and Cheung, H. C. (1986) *Biochemistry 25*, 6827−6835.
15. Ajtai, K., and Burghardt, T. P. (1995) *Biochemistry 34*, 15943−15952.
16. Strickland, E. H. (1972) *Biochemistry 11*, 3465−3474.
17. Goux, W. J., and Hooker, T. M. (1980) *J. Am. Chem. Soc. 102*, 7080−7087.
18. Park, S., Ajtai, K., and Burghardt, T. P. (1996) *Biophys. Chem. 63*, 67−80.
19. Tonomura, Y., Appel, P., and Morales, M. (1966) *Biochemistry 5*, 515−521.
20. Weeds, A. G., and Taylor, R. S. (1975) *Nature 257*, 54−56.
21. Ajtai, K., and Burghardt, T. P. (1992) *Biochemistry 31*, 4275−4288.
22. Werber, M. M., Peyser, Y. M., and Muhlrad, A. (1987) *Biochemistry 26*, 2903−2909.
23. Ellman, G. L. (1959) *Arch. Biochem. Biophys. 82*, 70−77.
24. Peyser, Y. M., Muhlrad, A., and Werber, M. M. (1990) *FEBS Lett. 259*, 346−348.
25. Borejdo, J., Putnam, S., and Morales, M. F. (1979) *Proc. Natl. Acad. Sci. U.S.A. 76*, 6346−6350.
26. Ajtai, K., Ilich, P. J. K., Ringler, A., Sedarous, S. S., Toft, D. J., and Burghardt, T. P. (1992) *Biochemistry 31*, 12431−12440.
27. Ajtai, K., and Burghardt, T. P. (1989) *Biochemistry 28*, 2204−2210.
28. Burghardt, T. P., Garamszegi, S. P., and Ajtai, K. (1997) *Proc. Natl. Acad. Sci. U.S.A. 94*, 9631−9636.
29. Hellen, E. H., Ajtai, K., and Burghardt, T. P. (1995) *J. Fluoresc. 5*, 355−367.
30. Schellman, J. A. (1975) *Chem. Rev. 75*, 323−331.
31. Bayley, P. M., Nielsen, E. B., and Schellman, J. A. (1969) *J. Phys. Chem. 73*, 228−243.
32. Goux, W. J., Radesch, T. R., and Hooker, T. M. (1976) *Biopolymers 15*, 977−997.
33. Goux, W. J., Cooke, D. B., Rodriguez, R. E., and Hooker, T. M. (1974) *Biopolymers 13*, 2315−2329.
34. Hsu, M. (1970) Optical activity of heme proteins.1−145. Thesis/Dissertation.
35. Grebow, P. E., and Hooker, T. M. (1975) *Biopolymers 14*, 871−881.
36. Yamaguchi, K., Tamura, Z., and Maeda, M. (1997) *Acta Crystallogr. C53*, 284−285.
37. Anderson, W. P., Edwards, W., and Zerner, M. C. (1986) *Inorg. Chem. 25*, 2728−2732.
38. van der Heide, U. A., Orbons, B., Gerritsen, H. C., and Levine, Y. K. (1992) *Eur. Biophys. J. 21*, 263−274.
39. Martin, M. M., and Lindqvist, L. (1975) *J. Lumin. 10*, 381−390.
40. Tinoco Jr., I., Ehrenberg, B., and Steinberg, I. Z. (1977) *J. Chem. Phys. 66*, 916−920.
41. Maita, T., Yajima, E., Nagata, S., Miyanishi, T., Nakayama, S., and Matsuda, G. (1991) *J. Biochem. 110*, 75−87.
42. Tong, S. W., and Elzinga, M. (1990) *J. Biol. Chem. 265*, 4893−4901.
43. Ramachandran, G. N., Ramakrishnan, C., and Sasisekharan, V. (1963) *J. Mol. Biol. 7*, 95−99.
44. Ramachandran, G. N. (1966) *Biophys. J. 6*, 849.
45. Strang, G. (1986) In *Introduction to Applied Mathematics*; Wellesley-Cambridge Press: Wellesley, MA, pp 87−137.
46. Borejdo, J., Ando, T., and Burghardt, T. P. (1985) *Biochim. Biophys. Acta 828*, 172−176.
47. Burghardt, T. P., and Ajtai, K. (1989) *Proc. Natl. Acad. Sci. U.S.A. 86*, 5366−5370.
48. Valeur, B., and Weber, G. (1977) *Photochem. Photobiol. 25*, 441−444.

49. Root, D. D., and Reisler, E. (1992) *Biophys. J. 63*, 730−740.
50. Jakob, U., Scheibel, T., Bose, S., Reinstein, J., and Buchner, J. (1996) *J. Biol. Chem. 271*, 10035−10041.
51. Burghardt, T. P., and Ajtai, K. (1996) *Biophys. Chem. 60*, 119−133.
52. Patterson, B., Ruppel, K. M., Wu, Y., and Spudich, J. A. (1997) *J. Biol. Chem. 272*, 27612−27617.
53. Shriver, J. W., and Sykes, B. D. (1982) *Biochemistry 21*, 3022−3028.
54. Ajtai, K., and Burghardt, T. P. (1986) *Biochemistry 25*, 6203−6207.
55. Bivin, D. B., Ue, K., Khoroshev, M., and Morales, M. F. (1994) *Proc. Natl. Acad. Sci. U.S.A. 91*, 8665−8669.
56. Phan, B. C., Cheung, P., Miller, C. J., Reisler, E., and Muhlrad, A. (1994) *Biochemistry 33*, 11286−11295.
57. White, H. D., and Rayment, I. (1993) *Biochemistry 32*, 9859−9865.
58. Highsmith, S., and Eden, D. (1993) *Biochemistry 32*, 2455−2458.
59. Wakabayashi, K., Tokunaga, M., Kohno, I., Sugimoto, Y., Hamanaka, T., Takezawa, Y., Wakabayashi, T., and Amemiya, Y. (1992) *Science 258*, 443−447.
60. Cheung, H. C., Gryczynski, I., Malak, H., Wiczk, W., Johnson, M. L., and Lakowicz, J. R. (1991) *Biophys. Chem. 40*, 1−17.
61. Mendelson, R. A., Schneider, D. K., and Stone, D. B. (1996) *J. Mol. Biol. 256*, 1−7.
62. Tesi, C., Barman, T., and Travers, F. (1988) *FEBS Lett. 236*, 256−260.

BI980015Y